RADIOHELIOGRAPH AND WHITE-LIGHT CORONAGRAPH STUDIES OF A CORONAL MASS EJECTION EVENT

N. GOPALSWAMY and M. R. KUNDU

Astronomy Program, University of Maryland, College Park, MD 20742, U.S.A.

(Received 9 May, 1988; in revised form 5 December, 1988)

Abstract. We analyze the radioheliograph and SMM-C/P observations of 1986 November 3 mass ejection event. The metric radio emissions are the only detected activity associated with the mass ejection, but are adequate to study the evolution of the event. The start time of the ejection seems to precede a possible flare behind the limb indicated by the early type III bursts. We discuss the physical relation between various types of bursts and the CME. We interpret moving type IV bursts as a plasma emission process. It is also shown using white-light coronagraph data that the density in the source region of the moving type IV is sufficient to support second harmonic plasma emission at the observed frequency of 50 MHz.

1. Introduction

Among a multitude of dynamical processes and activities in the solar corona, the coronal mass ejection (CME) has become a topic of primary interest over the past decade. It has become increasingly clear that the CME can not be studied in isolation because of its interaction with coronal structures such as streamers and its association with shock waves (manifested as type II bursts) and other moving entities such as plasmoids or magnetic arches (manifested as type IV bursts). CMEs have been extensively studied since their discovery in the early seventies. Radio bursts, especially type II and moving type IV bursts, on the other hand, have a much longer history. Unfortunately, only a handful of simultaneous observations of CMEs and radio bursts are available and, hence, a complete description of the CME-radio burst association is still lacking. Therefore, the study of individual events with simultaneous observations over a wide wavelength range is important for understanding the evolution of CMEs as a major component in a complex of dynamical processes. In this paper we present a study the of 1986 November 3 coronal mass ejection event which was observed both in white light by the SMM Coronagraph/Polarimeter and in radio by the Clark Lake multifrequency radioheliograph.

Although both the moving type IV bursts and the shock waves responsible for type II bursts propagate through the corona, with speeds often comparable to the CMEs, their exact physical relationship (e.g., the location of the radio sources with respect to the overall white-light transient event) is not fully understood. If the radio source is spatially coincident with the CME then the thermal electron density in the source can be derived from the white light data. This is a crucial paramter to understand the mechanism of radio emission. In the solar corona, nonthermal radio emission is generally believed to be caused by two processes: (i) plasma emission due to the conversion of longitudinal plasma waves (generated by a streaming or some form of unstable electron distribution)

Solar Physics **122** (1989) 145–173.

into propagating electromagnetic waves. This conversion may be through scattering on ion polarization clouds or on some low-frequency turbulence ('fundamental plasma emission') or by the coalescence of two high-frequency plasma waves ('harmonic plasma emission'); (ii) gyrosynchrotron emission from mildly relativistic particles as they spiral along magnetic fields contained in the source region. The plasma emission process depends upon the characteristics of the nonthermal electron distribution and the spectrum of plasma waves produced. The gyrosynchrotron emission depends on the distribution of both nonthermal particle density and magnetic field. The thermal plasma density plays a major role in determining the escape and propagation of the radio emission before it reaches the observer. If the generating mechanism is precisely known, the measured characteristics of the source such as brightness temperature, polarization, structure, etc., can be used to derive a number of macroscopic parameters in the source region. If scattering an refraction can be neglected, the plasma emission provides electron density because it is related to the observing frequency and can be compared with the density derived from the white-light observations of the associated CME. If the emission is due to gyrosynchrotron process, the white light estimates of density can be used to determine the extent of medium suppression (Razin effect) which in turn can be used to interpret the radio spectrum and derive, e.g., the magnetic field in the source (Gopalswamy and Kundu, 1987a).

Another important aspect of the CME-radio burst association is the acceleration of nonthermal particles responsible for the bursts. It is generally believed that there are two kinds of particle acceleration. One is the acceleration somewhere in the lower corona due to magnetic reconnection where the energy of the magnetic field annihilated in the current sheet is converted into particle energy. This type of acceleration is generally believed to be represented by hard X-ray, microwave and type III emissions and soft X-ray enhancements during the impulsive phase of flares and by the latter two in the absence of flares or in the preflare stage (Kundu *et al.*, 1988, and references therein). Electrons are also accelerated *in situ* in the front and wake of shock waves generated either by a flare explosion or by a CME moving with a super Alfvénic velocity. If the moving type IV bursts are physically associated with the CMEs then the question arises as to when and how the nonthermal particles find their way into the CME. It could be (i) during the precursor phase, (ii) the impulsive phase of the flare, if associated with CME, or (iii) from the shock formed ahead of the CME by virtue of its super Alfvénic motion. The observations of type III and type II bursts in association with the CME may clarify this point. The identification of the timing of acceleration is important in understanding the onset phase of the CME. There are several CME events whose onsets seem to be associated with weak soft X-ray brightenings that may or may not be followed by a flare (Harrison *et al.*, 1985). Type III bursts were also observed along with soft X-ray brightenings (Gopalswamy and Kundu, 1987a) implying particle acceleration during the onset phase of the CME.

The purpose of the present paper is twofold: (i) to discuss the observations in detail. The event originated from behind the limb and so most of the near-surface activities were occulted; however, we will demonstrate that various stages in the evolution of mass

ejection event can be understood using metric radio emission alone; (ii) to interpret the moving type IV bursts as second harmonic plasma emission which results in the estimation of macroscopic parameters of the source region.

2. Observations

The radio observations of the 1986 November 3 CME were made by the Clark Lake multifrequency radioheliograph (Kundu *et al.*, 1983) at three frequencies: 73.8, 50.0, and 38.5 MHz. The heliograph observations were made from 18:00 UT to ~ 22:30 UT and the nonthermal radio emission occurred between ~ 19:20 and ~ 20:30 UT. The white-light observations of the CME were made by the coronagraph/polarimeter aboard the Solar Maximum Mission satellite from ~ 19:21 UT until the end of the day. Hence, there is considerable overlap between the radio and white-light observations which enables us to compare the observations almost during the entire life time of the transient. We also made use of data from the Mark III *K* coronameter data from Mauna Loa and other information from *Solar Geophysical Data.*

2.1. Background to the Event

The event occurred above the NW limb of the Sun where there were two streamers, one close to the equator and the other at about 30° N. The equatorial streamer appeared dimmer than the northern one and probably was more radially behind the limb. The streamer structure was evident in the first SMM C/P picture at 19:21 UT, the Mark III *K* coronameter data, the Sacramento Peak coronal data and the coronal green line synoptic map. The radioheliograph data were sometimes noisy in the initial phase of the observations. During periods of low noise, extensions of the quiet-Sun limb were seen in correspondence with the white light streamers. Figure 1 shows the streamer structures from the Clark Lake Radioheliograph and MLO Mark III *K*-coronameter (see also Fig. 6). There was no surface activity or associated surface feature reported in *Solar Geophysical Data.* Active regions NOAA 4754 (S 04 W 12) and 4755 (N 01 W 07) were close to the disk center; they could not have produced the radio emission associated with the CME, as the radio sources were at a height of at least 2 $R_\odot$ from the disk center. These regions may have been responsible for a weak storm radiation which persisted with a brightness temperature of ~ 250 000 K throughout the observing period; the radio sources were always within the disk and were unaffected by the CME event (Figure 1). NOAA regions 4751 and 4752 probably had just crossed the limb by 1986 November 3 but they were in the southern latitude range of 17–24 and, therefore, could not have been associated with the CME. However, NOAA region 4750 had crossed the limb 2–3 days previously. This bipolar region was of relatively large extent (~ 25°) and was bisected by a filament; it produced several flares during disk passage. When region 4750 was on the western hemisphere, the Sacramento Peak coronal image showed growing streamer extension; the largest extension occurred when the region was on the limb (on 1986 October 31). On 1986 November 3, the region should have been ~ 30° behind the limb and it is possible that the mass ejection and

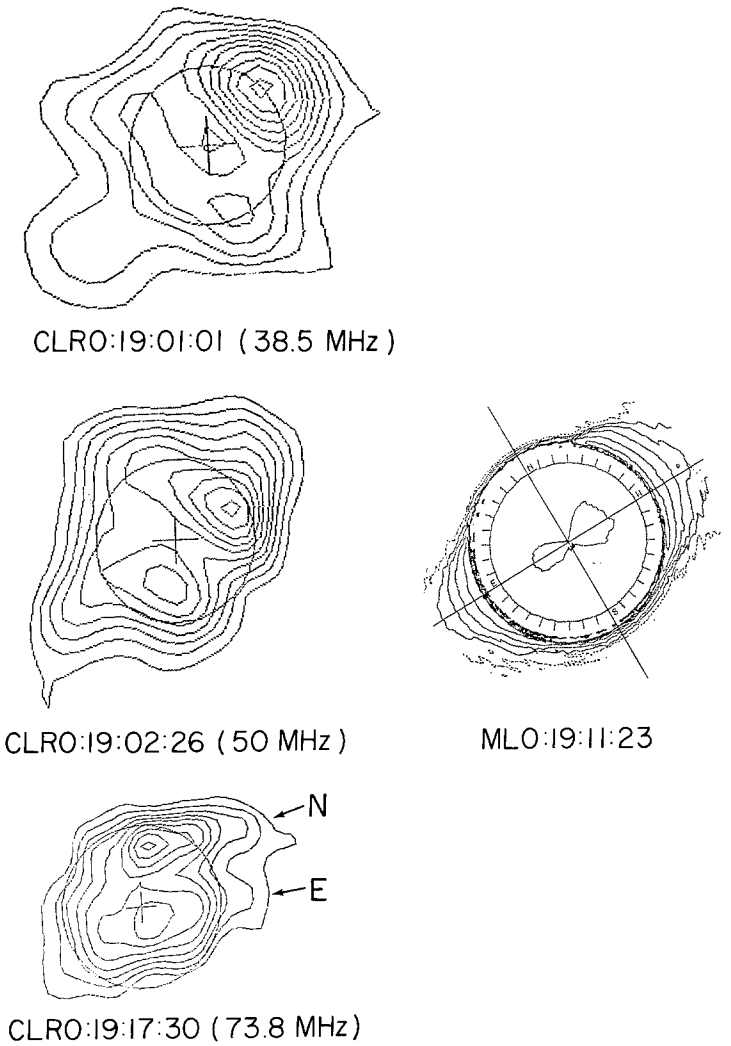

Fig. 1. Clark Lake radio maps at 38.5, 50, and 38.5 MHz and the Mauna Loa *K*-coronameter image showing the streamer structures. The streamer structure observed by SMM-C/P can be seen in Figure 6 (19:21 UT). The weak radio sources seen on the disk in the NW quadrant are due to a weak storm radiation. The northern (N) and equatorial (E) streamers are marked in the figure. The geocentric north is to the top and east is to the left.

the streamers were associated with this region. A prominence picture obtained towards the end of the CME event showed a prominence as a thin filamentary material rising above the chromosphere (McCabe, 1987, private communication). In order to be visible, the radial height of the prominence should have been at least 10^5 km which is not uncommon during prominence eruptions associated with CMEs (Schmahl and Hildner, 1977). Metric radio emissions have been observed in association with active regions $\sim 30°$ behind the limb (e.g., Kundu and Gopalswamy, 1987). Hence, we believe that the active region 4750 was probably associated with the 1986 November 3 CME.

2.2. Early type III bursts

The brightness temperature variation of the radio emission with time is shown in Figure 2. The event starts at ~19:20 UT with several sharp peaks at 38.5 MHz, while the increase is relatively smooth at higher frequencies. At each frequency, the emission builds up to a peak and then smoothly declines until ~20:40 UT. Higher frequency emission peaked earlier except for a steep rise at 38.5 MHz. Since Figure 2 shows only total brightness temperature, we used radio heliograms at various times to identify the various sources which contributed to the brightness temperature variation.

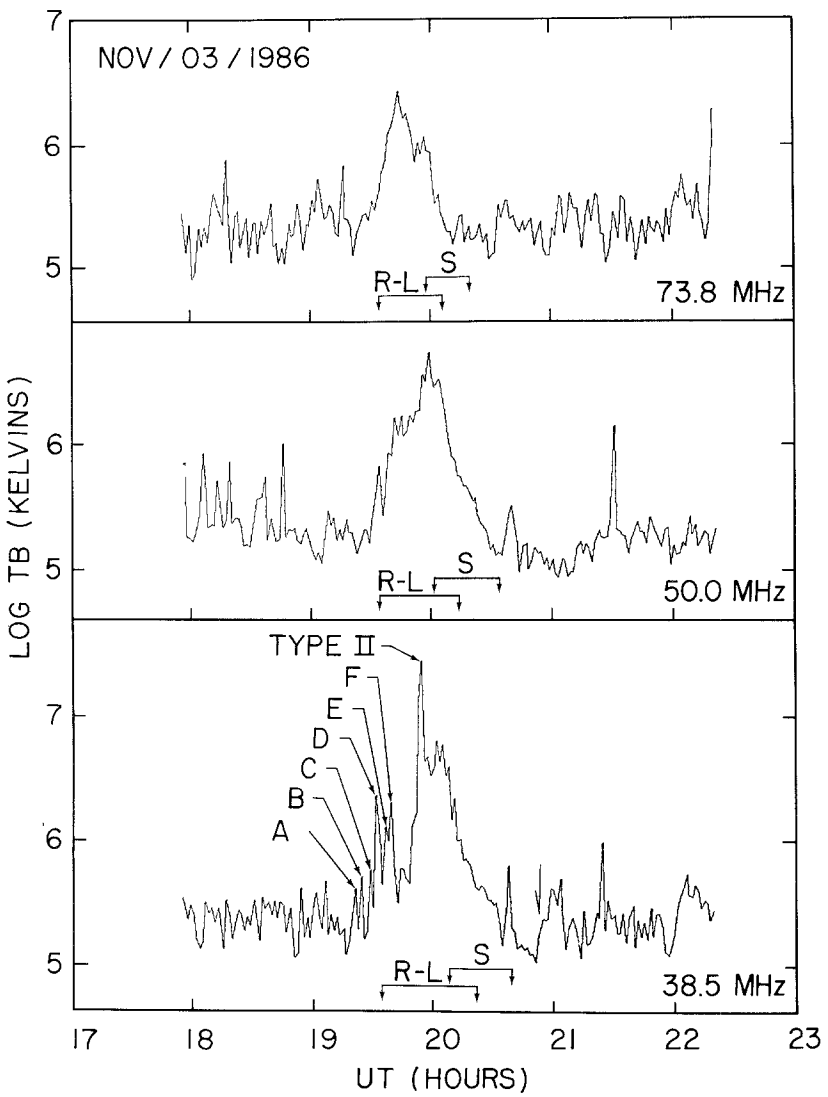

Fig. 2. Brightness temperature time plot of the radio emission on November 3, 1986. The early type III bursts are marked as the peaks *A*, *B*, *C*, *D*, *E*, and *F*. Type II burst is the largest peak seen at 38.5 MHz. The duration of the moving sources ($R - L$) and the quasi-stationary source (S) are marked in the figure.

During each of the first two peaks (marked *A* and *B* in Figure 2) there were two sources, one on the northern streamer and the other away northwards from the streamer as shown in Figure 3. Notice that the source on the streamer is at a larger height from the disk center compared to the other source. During both peaks, the 'on-streamer' sources were brighter and the brightness of the two sources were correlated despite their large separation of $\sim 1.6\, R_{\odot}$ at 38.5 MHz. Such correlated type III bursts have been

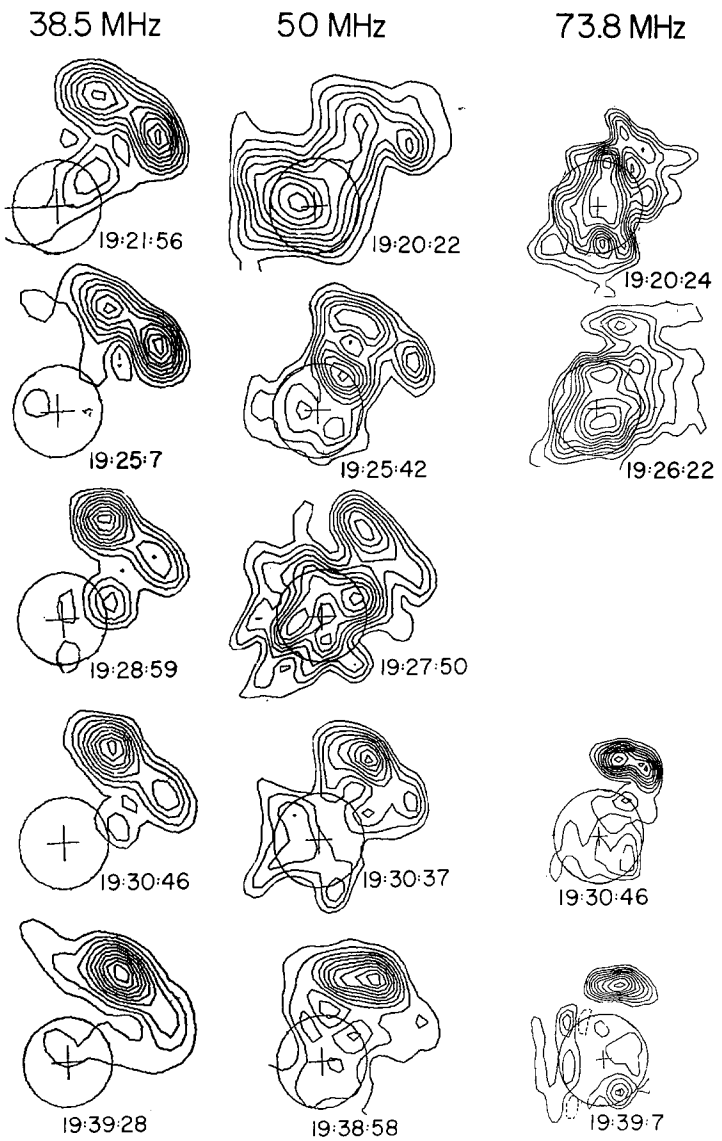

Fig. 3. Type III bursts which preceded the moving type IV bursts. The northern source is the 'off streamer' source and the western source is the 'on streamer' source. Notice that the western source is dominant in the top two panels (at 38.5 and 50 MHz). The type IV burst has already started at 50 and 73.8 MHz in the fourth panel whereas it starts only in the bottom panel at 38.5 MHz. Notice the double structure of the type IV burst at all frequencies in the bottom panel.

reported earlier (see e.g., Kundu and Gopalswamy, 1987). We believe that these are type III bursts indicating particle acceleration as early as $\sim 19:21$ UT. Figure 3 also shows that the type III emission probably was weak and close to the limit of detection at 50 and 73.8 MHz (see also Figure 2). Even during the later peaks (marked *C*, *D*, *E*, and *F* in Figure 2), the two sources were seen, but the 'off-streamer' source indicated the concentration of activity close to this source. Initially the 'off-streamer' source at 38.5 MHz was at a height of $\sim 2.6\, R_\odot$ and during the subsequent peaks the centroid moved slightly southwards and remained more or less stationary at a height of $\sim 2.35\, R_\odot$. The 'on-streamer' source also had a similar tendency and moved from a height of $\sim 2.77\, R_\odot$ to $2.5\, R_\odot$. Figure 2 shows that in addition to the peaks, the background emission also slowly built up which corresponds to the enhanced emission seen to the left of the 'off-streamer' sources in Figure 3.

2.3. Continuum and type II bursts

At the location of the off-streamer type III bursts, a continuum source appeared at $\sim 19:30$ UT at 50 and 73.8 MHz. This was the first bright source seen at these frequencies whereas the emission at 38.5 MHz could not be distinguished from type III emission. The source remained stationary for several minutes at all three frequencies. The sources started moving outward at $\sim 19:38$ UT at 50 and 73.8 MHz and around 19:40 UT at 38.5 MHz. As the sources moved, it became clear that they had double structure and the left-hand side (*L*) component was weaker than the right-hand side (*R*) one. The *R*-source appeared first at the location of the off-streamer type III. In fact, whenever the type III emission was low, the left-hand source was seen in the background at 38.5 MHz (see the 19:33 UT radio map in Figure 3). Once the motion started, the *L* soruce had almost the same brightness as the *R* source; at 50 MHz, the dominant emission flip-flopped between the *L* and *R* sources until 19:43 UT when the *L* source started dominating. The motion of the sources was not radial, but was slightly northward.

At 50 MHz, the separation between the *L* and *R* sources was $\sim 0.7\, R_\odot$ which appeared to diminish until 19:46 UT when a type II occurred as a discrete source in between but closer to the *L* source, and persisted for ~ 4 min. The type II was at a height of $\sim 2.3\, R_\odot$ with a peak brightness temperature (T_b) of $\sim 4 \times 10^6$ K. Figure 4 shows a set of radio maps before, during and after the type II burst at 50 and 38.5 MHz. Notice that the $L + R$ structure of the moving type IV source was seen at both frequencies before and after the type II. Following the appearance of the type II, two changes occurred: (i) the trajectory of the *R* source was deflected by more than $\sim 90°$ and its motion became almost radial, but the *L* source continued to move in the same direction as before; (ii) the *R* source brightness increased steadily and reached a peak T_b of $\sim 1.7 \times 10^7$ K (at 19:55 UT); within two minutes, the *L* source reached a peak T_b of $\sim 1.8 \times 10^7$ K (at 19:57 UT), although the increase in T_b was simultaneous in both sources. Following the peak of intensity in the *L* source, the *R* source again became dominant and continued to be so till the end. The $L + R$ separation at this time was $\sim 0.84\, R_\odot$ and continued to increase; it reached a value of $\sim 1.12\, R_\odot$ at 20:08 UT when

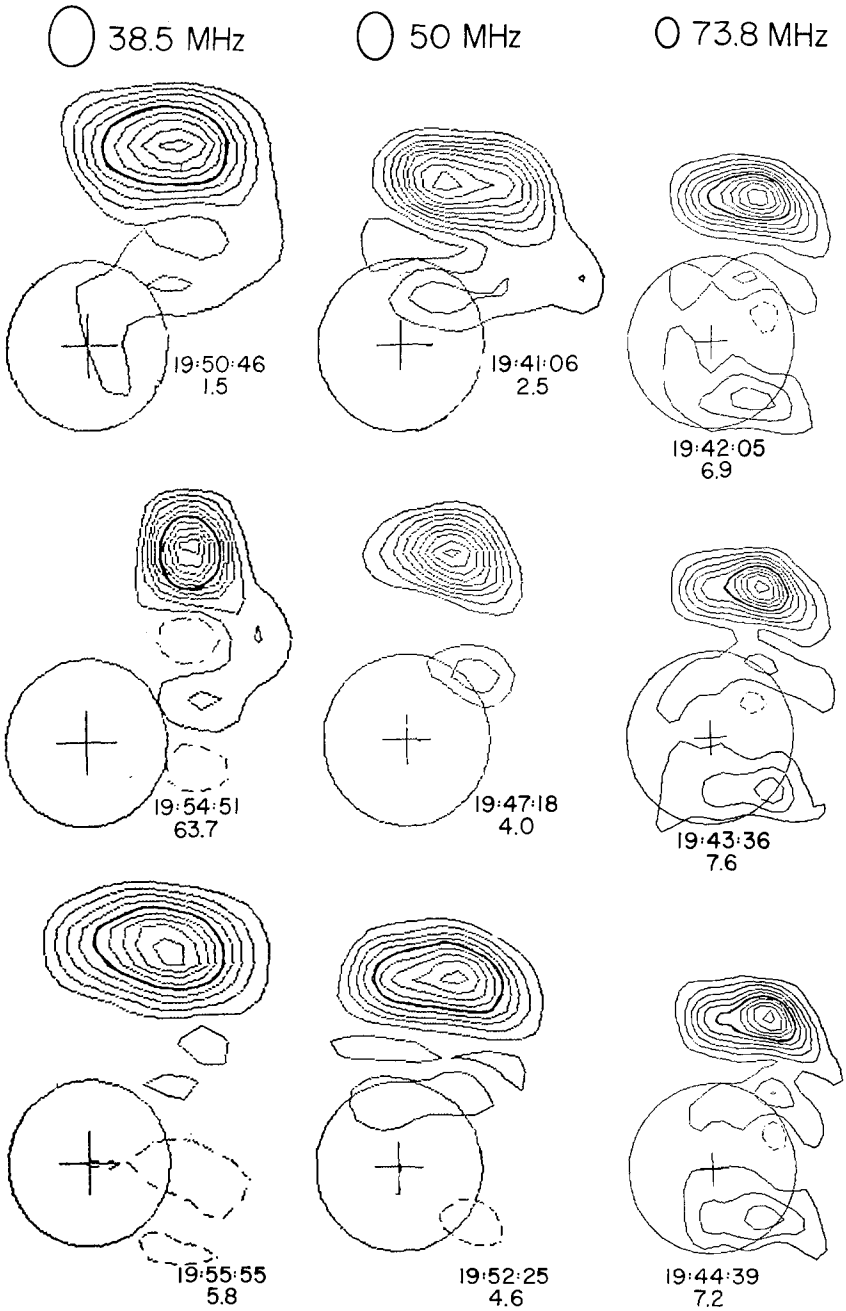

Fig. 4. The contour maps showing radio emission before (top panel) and after (bottom panel) the type II bursts (middle panel) at 38.5, 50 and 73.8 MHz. The time of the map and the peak brightness temperature (in units of 10^6 K) are marked near each map. Note the different location of the type II bursts at 38.5 and 50 MHz. At 73.8 MHz, the type II source is not seen distinctly, probably because it is weak. Geocentric north is to the top and east is to the left. The beam sizes at each frequency are marked at the top.

the L source faded below detection level. At 20:01 UT, a quasi-stationary type IV source developed in between but below the L and R sources at a height of $\sim 2.44\ R_\odot$ (the R source was at a height of $\sim 2.73\ R_\odot$). Interestingly, the R source also brightened from 6×10^6 K to 1×10^7 K. This new source remained quasi-stationary and persisted longer than the moving sources. The quasi-stationary type IV was seen distinctly at 20:06 UT and became dominant after 20:10 UT. The R source continued to decay and faded below the 15% peak T_b level of the stationary source and, therefore, could not be observed.

At 38.5 MHz the evolution was similar except that the L and R sources were observed as distinct sources only occasionally. The type II source occurred at 19:52 UT, well below the R source at a height of $\sim 2.6\ R_\odot$ and the moving source brightened following the type II and reached a value of $\sim 1 \times 10^7$ K. The type II burst at 38.5 MHz was the brightest source during the entire observation with a T_b of 6.4×10^7 K at 19:54 UT. This was observed as the largest peak in the T_b vs time plot (Figure 2). The trajectory change and the appearance of a quasi-stationary type IV followed at 19:56 UT and 20:08 UT, respectively, as in the case of 50 MHz.

At 73.8 MHz, the type II burst was not seen distinctly and it is not clear when it appeared; it is possible that it occurred at the same location as the R source, during its peak at 19:43 UT. The change in trajectory also is not very prominent but it can be seen from Figure 5(a) that the trajectory changed after the peak at 19:43 UT. The trajectory

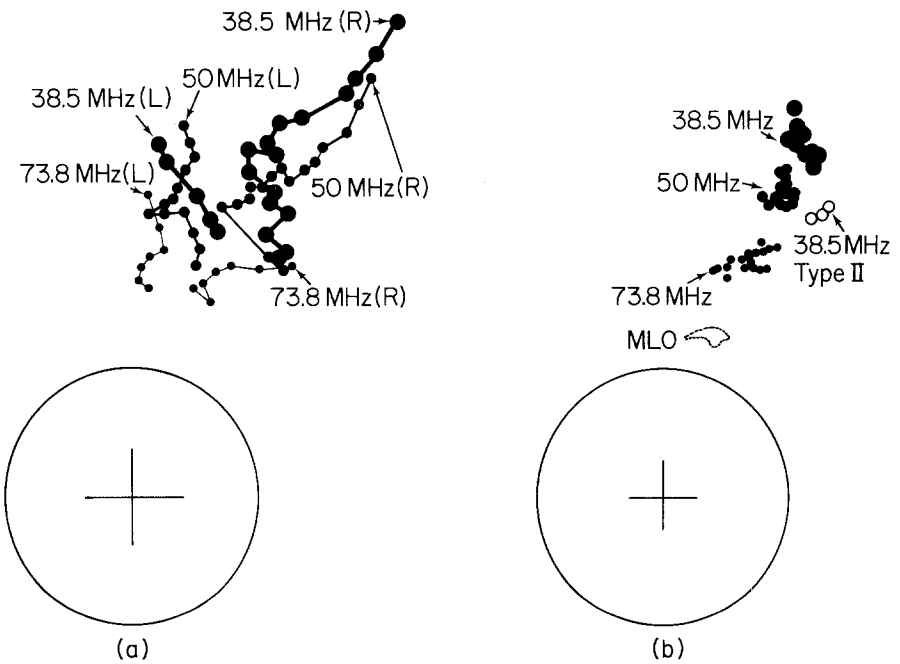

Fig. 5. (a) The centroids of the right (R) and left (L) leg sources of the moving type IV burst at 73.8, 50, and 38.5 MHz. The increasing size of the centroids correspond to the decreasing frequencies. (b) The centroids of the quasi-stationary type IV bursts at all three frequencies. The mass enhancement seen by the Mauna Loa Mark-III K-coronameter is shown by the dotted curve (MLO) at 20:01 UT.

almost made a U-turn and moved westward. The quasi-stationary source appeared again at a height of $\sim 1.71\ R_\odot$ between the $L+R$ sources. The moving sources faded much earlier at 73.8 MHz, and they were not observed beyond 20:02 UT. Table I summarizes the chronology of the type IV and type II burst appearance and their characteristics at the three frequencies. Table I shows that (i) the change in trajectory of the moving sources and the appearance of stationary type IV immediately follow the type II burst; (ii) the type II occurred close to or below the moving sources; and (iii) almost all bursts started and ended earlier at higher frequencies. Figure 5 shows the relative locations of various types of bursts.

TABLE I

Characteristics of radio emission at various stages

Event	73.8 MHz	50 MHz	38.5 MHz
Moving type IV			
Start time (UT)	19:30	19:30	19:30–19:40
Peak T_b (10^6) L/R	3.4/7.6	17.6/17.3	7.7/10.3
Time of peak (UT)	19:43:36	19:55:38–19:57:45	
Initial position ($R_\odot$) L/R	1.7/1.7	2.0/2.0	2.35/2.6
Final position ($R_\odot$) L/R	2.0/2.77	2.6/3.8	3.3/4.26
Last seen (UT) L/R	19:52:9/20:05:17	19:59:53/20:12:18	20:11:31/20:19:50
Type II			
Start time (UT)	19:43:36?	19:46:13	19:52:44
Location ($R_\odot$)	?	2.26	2.6
Peak T_b ($\times 10^6$ K)	7.6	4.0	63.7
Location of moving type IV R	1.9	2.27	2.71
End time (UT)	?	~19:50	~19:55
Trajectory change			
Start time	19:42	19:49	19:56
Height ($R_\odot$)	1.80	2.3	2.96
Position of moving type IV L/R	1.73/1.8	2.2/2.3	2.83/2.96
Stationary type IV			
Start time	19:52	20:01	20:08
Peak T_b ($\times 10^6$ K)	2.5	7.7	2.3
End time (UT)	29:17	20:29	20:35
Average height ($R_\odot$)	2.0	2.6	3.1

2.4. White-light observations

The SMM-C/P obtained white-light pictures of the event from ~19:21:03 UT to ~23:44:48 UT with three gaps of ~1 hr (Figure 6). The 19:21:03 UT picture shows the two streamers discussed earlier. In the picture at 19:39:47 UT a small loop shaped mass ejection appeared from the northern leg of the helmet streamer at a position angle of ~290°. The difference picture at 19:39:47 UT (from which the 19:21:03 UT picture has been subtracted) shows an almost semi-circular loop with legs separated by $\sim 0.8\ R_\odot$; the thickness of the loop was $\sim 0.3\ R_\odot$; the loop top was at a height of $\sim 2.4\ R_\odot$ from the disk center. The next picture at 20:36 after a gap of ~1 hr shows

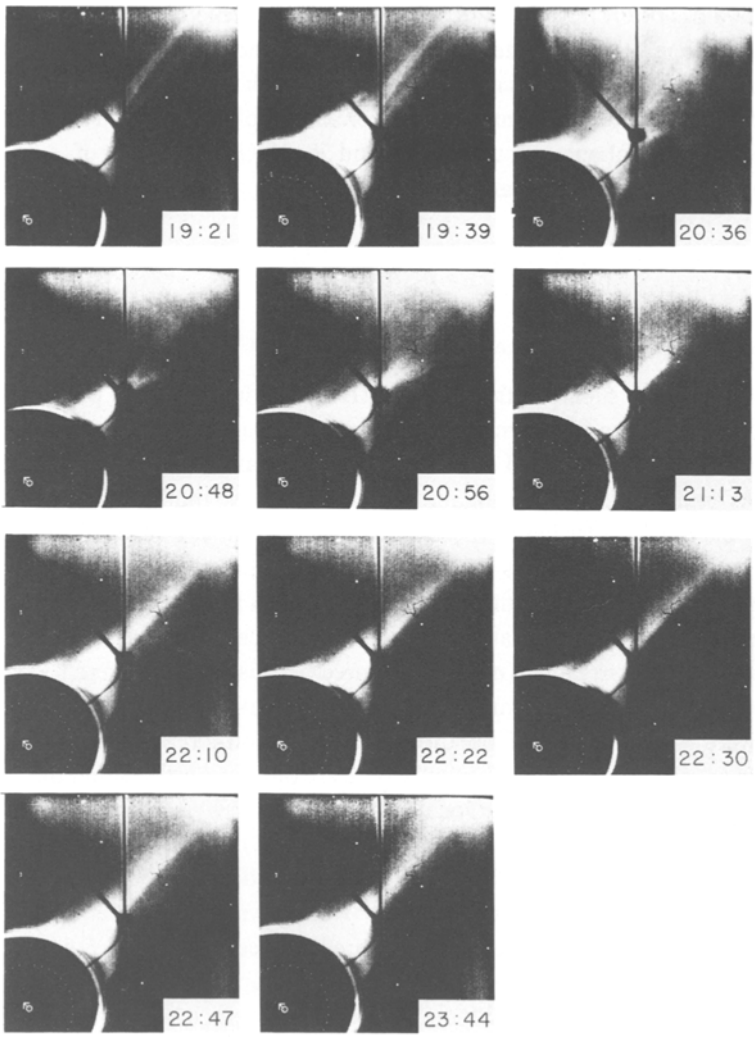

Fig. 6. Evolution of the white-light coronal mass ejection from 19:21 to 23:44 UT. The mass ejection was first seen at 19:39 UT. The arrow marks indicate solar north.

that the northern streamer was completely disrupted and the ejected material almost filled the field of view from position angle of $\sim 255°$ to $\sim 320°$. The presence of the weak equatorial streamer makes the picture quite complex. It gives the appearance of two diffuse loops, one to the north and the other to the south of the disrupted streamer. The northern loop appears to have expanded from the loop seen initially at 19:39:47 UT. The loop top must have moved to the edge of the field of view at 20:36 UT and, therefore, we could not measure the speed of the CME accurately. From the images at 19:39 and 20:36 UT, the lower limit to the speed is ~ 525 km s^{-1}.

The picture at 20:48 UT shows that the equatorial streamer was also deflected southward, and it slowly recovered after 20:56 UT and was restored to the original

shape by $\sim$22:10 UT. At 23:44 UT, the streamer structure looked similar to the pre-event configuration but the central ray of the northern streamer was missing. Throughout the event there was remnant material which was observed as faint expanded legs of the initial loop. The Mark III *K*-coronameter of Mauna Loa Observatory also showed brightness enhancements at 20:01 and 20:20 UT at a height of $\sim 1.4\ R_\odot$ which might correspond to the remnant material.

3. Analysis

3.1. Association of radio and white-light sources

Figure 7 shows the superposition of type III bursts in the initial phase, the moving sources and the stationary sources at three frequencies on the C/P images. The location of on- and off-streamer type III sources at 19:21 UT are shown in Figure 7(a). Radioheliograms and Mark III *K* coronameter pictures show that the base of the helmet streamer was much wider below the occulting disk of the C/P. Therefore, the northern ('off-streamer') type III sources might be located on the open field lines bordering the helmet streamer while the southern source may be on the streamer field lines. This is further supported by the fact that the on-streamer source (southern) is at a greater height compared to the off-streamer (northern) source because of the different densities and correspondingly different plasma levels at these locations. At 50 MHz, the type III sources were weaker but still show the same on- and off-streamer characteristics. The 73.8 MHz sources were still weaker, and there are only suggestions that the bursts must have occurred at the appropriate locations.

Figure 7(b) shows the moving sources (both *R* and *L*) superposed on the loop-shaped CME. At 73.8 MHz, the centroid of the radio source does not coincide with the CME loop. However, the half-power contours do overlap with the northern leg of the loop. The centroid of the radio source may be located between the *R* and *L* sources because of their equal brightness and, therefore, the *R* source appears to be associated with the brighter northern leg of the CME loop. This is clearly seen in the 50 MHz map. In this case, the *R* source is located exactly at the center of the northern leg, but the *L* source is located northward away from the leg. Notice also the lower height of the *L* source. At the level of 35% of the peak T_b the *R* source contours seem to lie on the southern leg of the loop. There is a slight radio brightness enhancement beyond the southern leg of the CME loop, where the streamer is located. The 38.5 MHz radio source is not resolved but still shows the centroid associated with the northern leg of the CME loop. Note that most of the 73.8 MHz moving source is still below the occulting disk of the SMM-C/P. Even the lower frequency sources have not moved beyond the occulting disk completely. Ionospheric effects were present as a smooth sinusoidal variation superposed on the height-time curve with a period of $\sim$15 min. This was probably due to gravity waves. Clear peaks were seen at 19:46, 20:00, 20:14, and 20:26 UT at all three frequencies. The amplitude of the ionospheric variation follows the familiar inverse frequency-square law. The 38.5 MHz height variation has a maximum amplitude of $\sim 0.35\ R_\odot$. The amplitude is much less than the beam size at both 73.8 and 50.0 MHz.

This variation is small compared to the overall extent of source motion which was $\sim 2.0\ R_{\odot}$. Note that 19:39 UT does not lie on the peak of ionospheric cycle and, hence, to displacement of the radio source from the white-light features may not be due to the ionospheric refraction. Coronal refraction and scattering might have played some role.

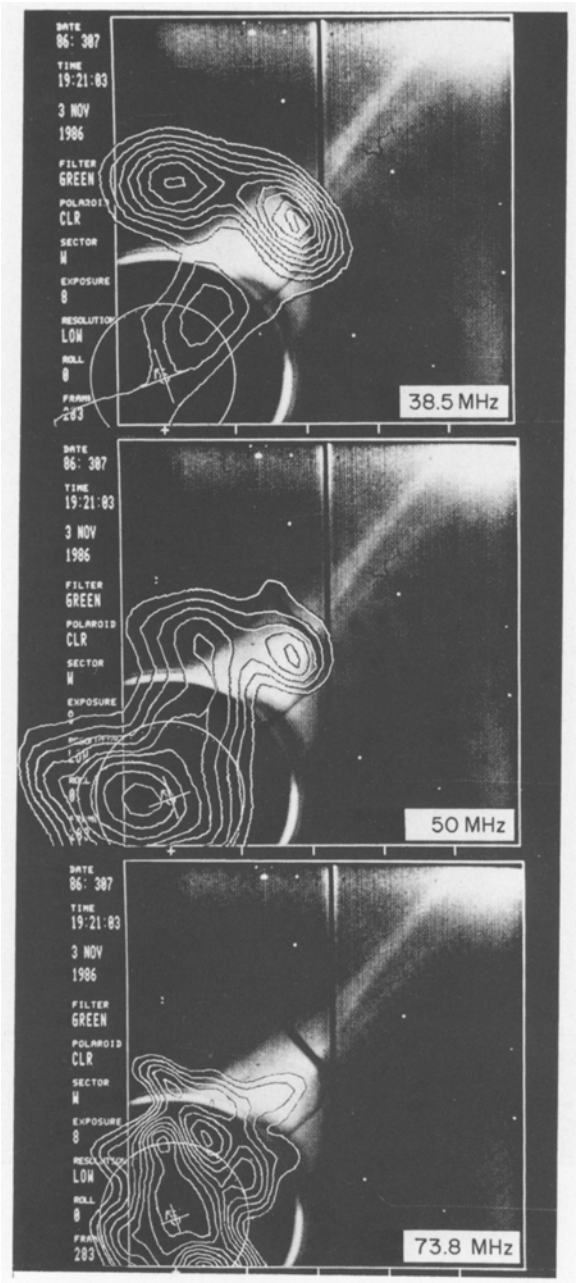

Fig. 7a.

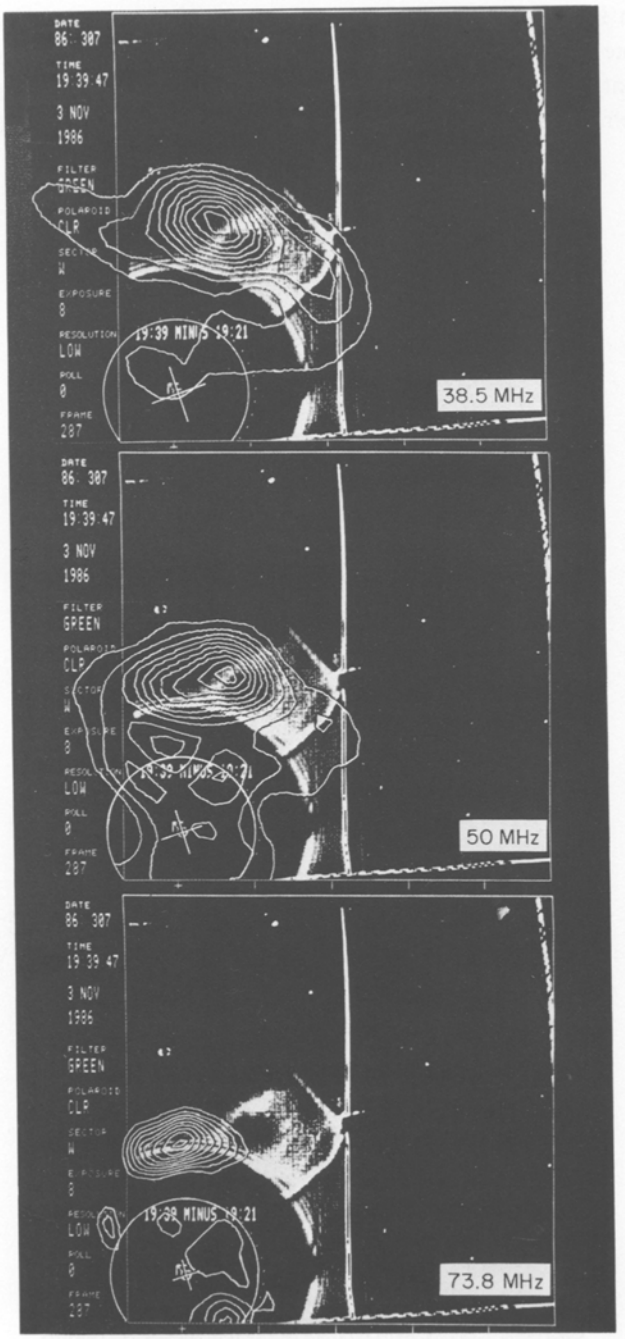
DATE
86: 307
TIME
19:39:47
3 NOV
1986
FILTER
GREEN
POLAROID
CLR
SECTOR
W
EXPOSURE
8
RESOLUTION
LOW
POLL
0
FRAME
287
19:39 MINUS 19:21
38.5 MHz
50 MHz
73.8 MHz

Fig. 7b.

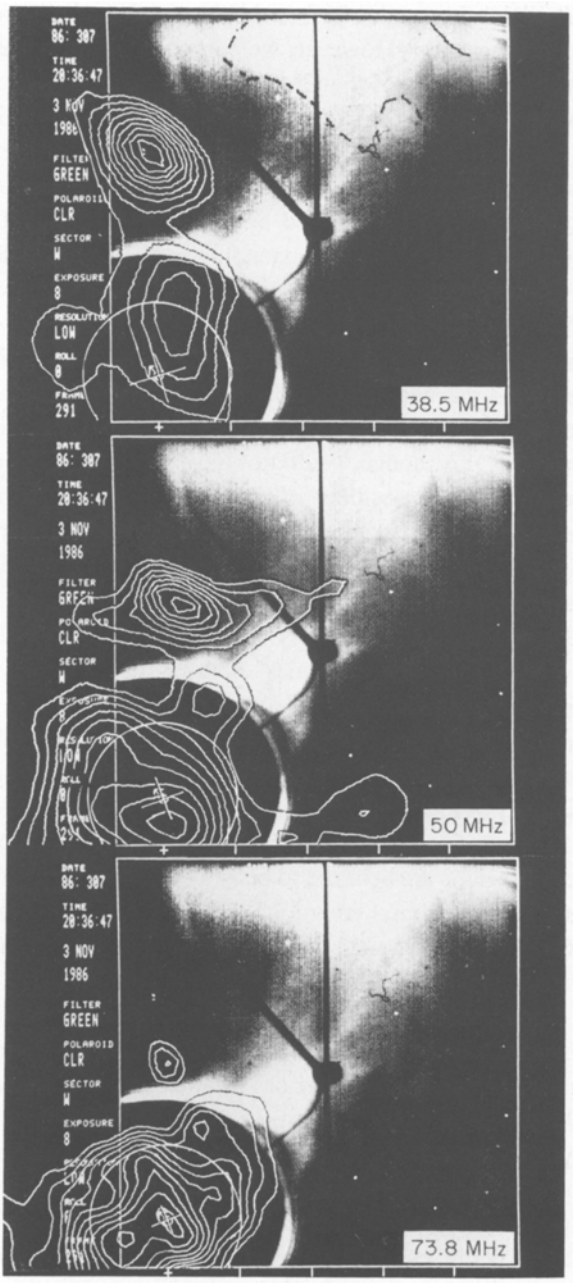

Fig. 7c.

Fig. 7. Superposition of radioheliograms at 73.8, 50, and 38.5 MHz on the CMM-C/P images at various stages. (a) Association of type III bursts with the streamers observed by SMM-C/P. (b) Location of moving type IV bursts relative to the white-light transient. The SMM-C/P difference picture is obtained by subtracting the 19:21 UT (pre-event) image from the 19:39 UT image. (c) Location of the quasi-stationary type IV bursts relative to the white-light transient at 20:36 UT.

As there is no white-light observation before the decay of moving type IV, it is difficult to come to any firm conclusion. However, we can conclude that the radio activity is centered around the brighter leg of the CME loop.

Figure 7(c) shows the relative location of the quasi-stationary radio source and the expanded CME. Although the CME covers almost the entire field of view, the radio sources are still confined to the north-western quadrant only. The quasi-stationary sources are located close to the expanded northern leg of the CME loop while the 50 MHz maps still show radio contours extending to the southern leg.

3.2. Plasma levels of the undisturbed corona

As mentioned earlier, the background density is one of the crucial parameters in determining the emission mechanism for radio sources. The positional observations of type III bursts can be used to determine the background electron density (Gopalswamy, Kundu, and Szabo, 1987). Although we do not have good temporal resolution for the present set of observations, the positions of type III bursts are known. To convert the type III source heights into plasma levels we need to decide whether the type IIIs are due to fundamental (F) or harmonic (H) plasma emission. We believe that the type IIIs in the present case are due to H emission for the following reasons.

(i) The average heights of type III sources from the disk center are 2.2 (1.7), 2.4 (2.0), 2.6 (2.4) $R_\odot$ for on-streamer (off-streamer) sources at 73.8, 50, and 38.5 MHz, respectively. These heights could be $\sim 15\%$ more if associated with the active region $\sim 30\%$ behind the limb. Assuming that scattering and ducting are small at least at higher frequencies, these heights are too large for the fundamental emission. The coronal background density may be approximated by the Baumbach–Allen (B–A) model if there are no structures present. On the streamer axis, Newkirk's model may be used. The densities above active regions are believed to be ~ 5–7 times more than the background density. If we assume fundamental emission, and fit the off-streamer burst heights to the B–A model, we need to use 10–20 times the B–A model, whereas 2.5–6 times the B–A model fits the H emission. For the on-streamer bursts, the H emission fits the 3-times Newkirk streamer model while the F emission needs a multiplicative factor of ~ 15. Both these estimates indicate that the H emission is more appropriate. It must be pointed out that scattering and ducting of radiation can affect the observed heights (e.g., Duncan, 1979), which is more severe for fundamental emission.

(ii) Statistically it is known that type III bursts occurring close to the limb are predominantly due to harmonic emission and the F emission is not observed apparently due to its high directivity (Suzuki and Sheridan, 1982). Suzuki and Dulk (1985) have also shown that the 'structureless' type III bursts are observed more frequently near the limb and always have the characteristics of harmonic emission.

Since most of the radio activity is confined to the region away from the streamer, we assume that the background density follows the B–A model multiplied by a factor of 4 (obtained from fitting burst heights to the model). The 4 times B–A model is used to derive the heights at which 73.8, 50, and 38.5 MHz plasma levels occur as 1.78, 1.63, and 1.44 $R_\odot$ from the disk center. As there was no white-light transient above the

occulting disk (at a height of $\sim 1.5\, R_\odot$) at the time of type III bursts, these estimates of plasma levels should represent the undisturbed corona.

3.3. HEIGHT-TIME ANALYSIS

The measured heights of various sources from the disk center are plotted in Figure 8 against time at all three frequencies. The height time plot can be divided into four parts: (i) 19:21 to 19:30 UT, during which only the type III bursts occurred; (ii) 19:30 to

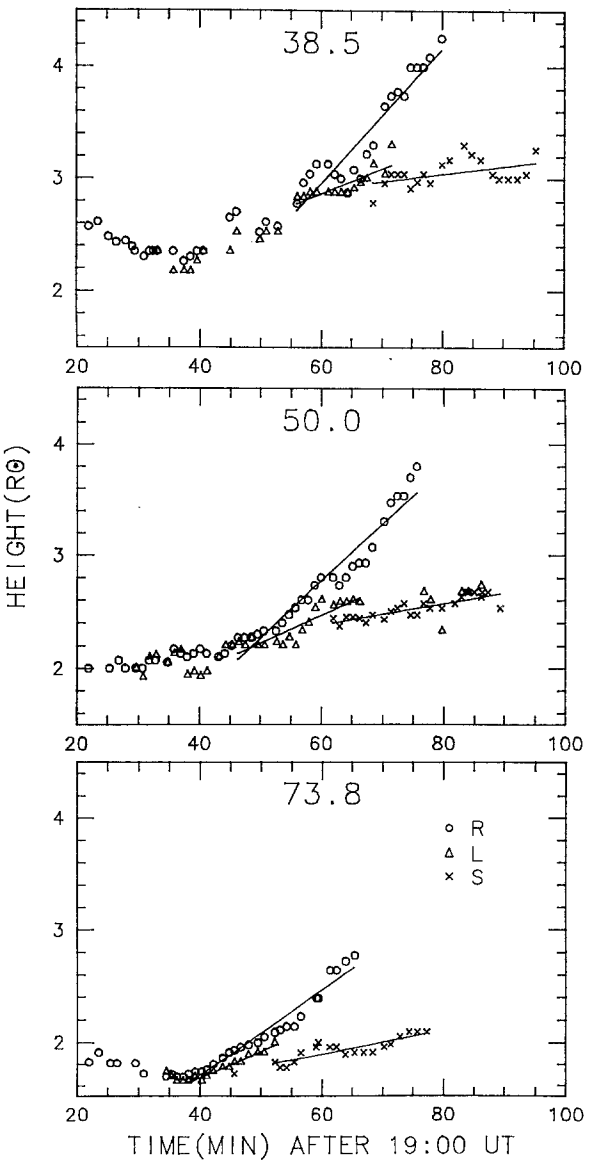

Fig. 8. Height-time plot of the R, L, and S sources at 73.8, 50, and 38.5 MHz. The early type III bursts (off-streamer) are also marked as R because they occurred at the location of R. The solid lines are the least-square fits to the height variation.

19:38 UT, during which mostly the R source was dominant and stationary at the location of type III bursts; the L source became visible toward the end of this interval; (iii) 19:39 to 19:55 UT, during which the trajectory of the sources was non-radial and the slope of the height time plot was smaller, and (iv) 19:55 UT onwards, during which the motion of the sources became almost radial. The changes in trajectory and the stationary type IV source occurred at 50 and 38.5 MHz in this interval.

Linear fits to part (iv) of the height time plot indicate speeds of 445, 590, and 700 km s^{-1}, respectively, for the 73.8, 50, and 38.5 MHz R sources while speeds for the L source are smaller: 290, 280, and 260 km s^{-1}. The large dispersion in the speeds of the R sources stem from the fact that at 73.8 and 38.5 MHz the R source has considerable non-radial motion. At 38.5 MHz, the ionospheric modulation might also have influenced the height time variation. The average speed of the R source is ~ 580 km s^{-1}. The speed of the L source is $\sim$ half of the R source speed at all frequencies. This may be due to the motion being away from the plane of the sky. Recall that the lower limit to the speed of the CME is ~ 525 km s^{-1}. This is close to the average speed of the moving type IV. It is conceivable that the moving type IV bursts occurred in closed magnetic fields which moved out in association with the CME. The 'stationary' sources show a slight outward motion with a similar speed (in the range 80–115 km s^{-1}) at all three frequencies. This motion may be due to the displacement of the remnants behind the CME. Similar motion in a quasi-stationary type IV has been reported by Gary *et al.* (1985).

The double structure of the moving sources and the non-radial motion can be better understood from Figure 9. In order to illustrate the relative positions of the sources at various frequencies, we have connected the L and R sources and we find that they lie along the two legs of a giant arch which expands in time. Initially the separation between the legs of the arch is small, and it increases with time. Both L and R sources show a systematic dispersion of source positions along their respective legs. A most striking observation is the tilt of the axis of the arch northwards from the initial position. At 19:50 UT, the axis almost becomes radial and the type II burst occurs close to this time at 50 and 38.5 MHz. Notice that the 50 MHz type II burst is located in between the legs while the 38.5 MHz type II source is located at the right-hand side of the right leg. This may be related to the fact that both L and R sources brightened following the type II burst at 50 MHz. The 73.8 MHz stationary type IV also occurs at this time and is located in between the two legs, on the axis of the arch. Following the type II burst, the axis tilts further to the north and remains almost the same from $\sim$ 19:55 UT till the end of the burst. In the Figure 9(k) we have sketched the loop through the sources from $\sim$ 20:06 to 20:19 UT, the last time the moving source was seen. Notice again the position of the quasi-stationary sources dispersed in frequency along the axis of the arch.

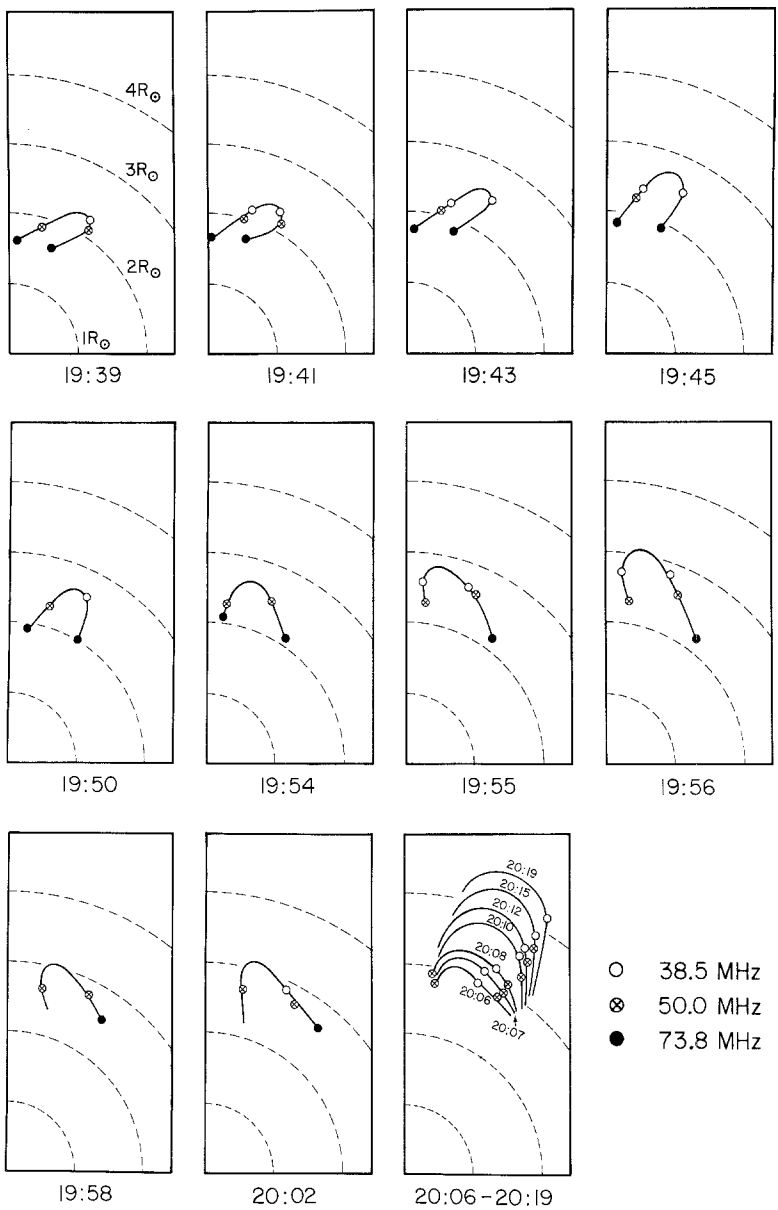

Fig. 9. Evolution of the centroids of the moving type IV bursts along the legs of a huge arch. The arch is drawn through the L and R source centroids at all three frequencies. The disk center is at the lower left corner of each box. The dashed curves represent heights in units of solar radii from the disk center as marked in the top left box. In the last box, we have drawn all the loops corresponding to the period from 20:06 to 20:19 UT.

4. Discussion

4.1. Initial particle acceleration

To understand the evolution of the radio emission, we need to know the origin of nonthermal particles and the mechanism by which they emit various types of bursts. The earliest activity is the type III emission (19:21 UT) in the undisturbed corona and there were no white light activity at this time. The type III bursts are known to be generated by streams of electrons of energy $\gtrsim 10$ keV accelerated low in the corona. As these streams have high velocity ($\sim 0.3c$), they take only a few seconds to reach the decametric corona to produce the observed emission. The mass ejection and the shock waves travel more slowly compared to the type III emitting electrons and so they would take much longer time to reach the same level even though the latter might originate at the same time and location as the type III electrons. Hence, we may expect that the type III burst onset indicates the start of the event more accurately than the other emissions, or at least indicates the onset of electron acceleration process. Type III bursts occur both during the precursor and the impulsive phases of flares (see e.g., Kundu *et al.*, 1988; Gopalswamy and Kundu, 1987b). The initial stationary phase of the moving sources follows the type III bursts. Further, the initial location of the moving burst is the same as that of the type III bursts. The stationary phase of the moving sources (R and L) is very similar to the early flare continuum (FCE) discussed in detail by Robinson (1985). The type III stationary phase combination is very similar to the type III-FCE combination of the February 3, 1986 flare discussed by Gopalswamy and Kundu (1987b), in that the $R+L$ sources occur in closed magnetic fields and the type III occurs in open magnetic field lines. This suggests that the magnetic field lines on which the $R+L$ sources (closed) and type III bursts (open) occur must share the same acceleration region. Therefore, the stationary phase of the $R+L$ sources appears to be similar to a flare continuum occurring on the two legs of a magnetic arch which eventually moves outward and becomes the moving type IV burst. There is no short wavelength radio, optical or X-ray activity associated with this event. This is expected because the associated active region was $\sim 30°$ behind the limb, and all these emissions would have been occulted. Therefore, we believe that an acceleration process such as a flare must have occurred behind the limb during the type III-FCE phase and must have supplied the necessary nonthermal electrons to generate these radio bursts. The simultaneous occurrence of 'on-streamer' type III bursts separated by distances $\sim 1.6\, R_\odot$ from the off-streamer type III, FCE bursts indicates again a common acceleration region low in the corona, as shown by Kundu and Gopalswamy (1987).

4.2. Type II–moving type IV connection

The significant brightening of the moving sources is seen immediately after the type II burst. This suggests an additional supply of high energy electrons to the arch as the type II shock sweeps through the arch. As there is no spectrographic information, it is difficult to calculate the speed of the type II shock. However, we can estimate it based on the time of arrival of the shock at various heights as observed at 38.5 and 50 MHz.

The type III bursts are prompt indicators of impulsive phase of the flare. Therefore, we may assume that the type II shock also started at the time of occurrence of the first type III burst (19:21 UT). We take the shock arrival times at heights of 2.3 and 2.6 $R_\odot$ to be 19:46 and 19:52 UT as observed at 50 and 38.5 MHz, respectively. As the flare is believed to occur at a height of $\sim 10^4$ km above the photosphere (de Jager, 1986), the speed of the type II shock becomes ~ 650 km s^{-1}. It is to be noted that the type II burst was located very close to the 50 MHz moving source and $\sim 0.3\,R_\odot$ behind the 38.5 MHz moving source. Therefore, the type II burst certainly did not occur ahead of the moving source as one would expect if the type II burst was generated by a piston driven shock located at the 'stand-off' distance ahead of the CME. Let us compare the dynamics of the moving source with that of the type II shock. It is now clear that the CME lifts off several minutes before the associated flare (see, e.g., Wagner, 1985; Harrison *et al.*, 1985). The moving type IV arrives at heights 2.0 (50 MHz) and 2.6 $R_\odot$ (38.5 MHz) at 19:30 and 19;38 UT (see Table I). As the average speed of the moving source is ~ 580 km s^{-1}, the CME might have left the surface between 19:06 and 19:10 UT which is ~ 13 min before the flare start, consistent with the fact that CME onset is several minutes before the flare start. Since the speed of the moving type IV burst is about the same as that of the shock, we expect the type II location behind the type IV at a distance of $\sim 0.7\,R_\odot$. But the observations show that the type II is $\sim 0.3\,R_\odot$ behind type IV at 38.5 MHz and close to type IV location at 50 MHz. It must, however, be remembered that initially the motion of type IV was non-radial and so the radial distance travelled was smaller. The type II might have caught up with the type IV during this period. In other words, the trajectory of the moving type IV and type II shock may not be the same. In summary, the type II burst appears to be generated independent of the moving type IV burst and might have been due to the flare as reported earlier (Wagner, 1985; Gopalswamy and Kundu, 1987a, and references therein).

4.3. The stationary type IV burst

Observations presented in Figure 5 clearly shows that (i) the quasi-stationary type IV bursts are associated with the interior region behind the CME; (ii) the bursts have a small speed of ~ 100 km s^{-1} implying the continued slow evolution of the corona behind the CME; and (iii) the burst sources at three frequencies have a clear dispersion with a separation $\sim 0.6\,R_\odot$ and $\sim 0.5\,R_\odot$ between 73.8 and 50 MHz and 50 and 38.5 MHz centroids, respectively; the columnar structure is further verified by the enhancement seen by the MLO *K* coronameter data (Figure 5(b). It is interesting to note that the quasi-stationary type IV is similar, in many respects, to the type IV burst reported by Gary *et al.* (1985).

4.4. Gyrosynchrotron versus plasma emission

The FCE emission is believed to be due to second harmonic plasma emission. While the plasma emission mechanism is accepted for most of the non-moving bursts such as type III, type II, and even stationary type IV bursts, gyrosynchrotron emission is believed to operate in moving type IV sources. The main objection to the gyro-

synchrotron emission is the high brightness temperature observed in the early phase of some events. Brightness temperatures as high as 5×10^{12} K have been observed (Duncan 1981) which demand unrealistically high energies for the nonthermal electrons if they are to be explained in terms of gyrosynchrotron emission. Such high brightness temperatures can be more easily explained in terms of second harmonic plasma emission. The polarization behavior during the late phase of type IVs seems to favor gyrosynchrotron emission. A combination of these two processes seems to be a possibility (Melrose, 1980). In the gyrosynchrotron theories, the source is a plasmoid and all frequencies are assumed to emanate from the same location. In other words, it is believed that no systematic dispersion of source position with frequency exists. However, Duncan (1981) presented evidence for systematic dispersion of source position for several moving type IV events. Since this is a characteristic for all plasma emissions, Duncan concluded that moving type IV bursts could be explained by plasma emission process. Recent coronagraph observations indicate that density enhancement by a factor of ~ 40 could occur in the corona in CMEs which is sufficient to allow plasma emissions at great heights in the corona (Stewart *et al.*, 1982).

In the present observations, the peak brightness temperature never exceeds $\sim 1.8 \times 10^7$ K. From Table I we see that the peak brightness temperature of the moving type IV burst is maximum at 50 MHz ($\sim 1.8 \times 10^7$ K) and decreases both at higher (73.8 MHz: $T_b \sim 3 - 8 \times 10^6$ K) and lower (38.5 MHz: $T_b \sim 8-10 \times 10^6$ K) frequencies. This means that the peak emission frequency is somewhere around 50 MHz. If the emission is due to gyrosynchrotron process from power-law electrons, then at 50 MHz the optical depth is ~ 1 and the lower frequency (38.5 MHz) emission must be optically thick while at the higher frequency (73.8 MHz) the emission must be optically thin. For optically thick gyrosynchrotron emission, the effective temperature of the emitting electrons is nearly the same as the brightness temperature, viz., 1.8×10^7 K, which corresponds to an electron energy of ~ 1.5 keV. For the 38.5 MHz emission, $T_b \sim 10^7$ K, so that the electron energy is ~ 1 keV. We need not consider Razin suppression in estimating the effective temperature as the brightness temperature at 38.5 MHz is not too low compared to the peak brightness temperature. The lifetime (τ) of such low-energy electrons trapped in a magnetic arch is rather low, because

$$\tau = 2.0 \times 10^8 n_0^{-1} E^{3/2} \text{ s}, \tag{1}$$

where E is the electron energy in keV and n_0 is the density of background electrons (Melrose and Brown, 1976). As the Razin suppression is not significant, the density in the source region has to be such that the plasma frequency does not exceed one half of the observing frequency (e.g., Melrose, 1980). For an observing frequency of 50 MHz, let us assume that the background electron density in the source corresponds to a plasma frequency of ~ 25 MHz, so that $n_0 \simeq 7.5 \times 10^6$ cm^{-3}. (This is indeed the case, as will be shown below using white-light observations.) Using $E_0 \sim 1.5$ keV obtained above, we see that $\tau \sim 40$ s. As the lifetime of the moving type IV bursts is $\gtrsim 45$ min, the low-energy electrons could not have produced the observed emission. The energy of the electrons may not be so low from another point of view: the type III bursts which

preceded the moving type IV indicate the presence of nonthermal electrons with energies in the range 3–50 keV (Lin *et al.*, 1981). The electrons causing moving type IV may also have similar energies if they have a common source of acceleration. While both low- and high-energy electrons can escape along open field lines causing type III bursts, the lifetime of low-energy electrons is short when they are trapped as indicated by the relation (1). If $E_0 \sim 25$ keV, we see that $\tau \sim 55$ min, which is in the range of observed lifetime of moving type IV bursts. Another possibility is optically thick gyroresonance emission due to a quasi-thermal population of electrons with a temperature of $\sim 1.8 \times 10^7$ K. Calculations by Gary *et al.* (1985) for this brightness temperature range show that an unrealistically high magnetic field is needed. Therefore, a plasma emission process seems to be likely. Moreover, the clear arch structure and high dispersion of source positions (Figure 10) lead us to believe that the moving type IV burst in the present case may be due to plasma emission.

The low brightness temperature ($< 2 \times 10^7$ K) is to be explained in terms of plasma wave generation processes and their conversion into observable radiation. Melrose (1975) pointed out that brightness temperatures as low as $\sim 10^6$ K could result at ~ 100 MHz due to the coalescence of plasma waves generated by isotropic electron distributions. Estimates at meter-decameter wavelengths show that such an isotropic distribution may not produce observable radiation. Brighter emission needs some sort of anisotropy in the nonthermal electron distribution. We discuss a loss-cone anisotropy in the following section which appears most appropriate for the present event.

4.5. Plasma emission mechanism for moving type IV bursts

The theory of moving type IV bursts based on second harmonic plasma emission was originally developed by Stepanov (1974). Energetic electrons trapped in a magnetic loop have a loss-cone distribution which excites plasma waves near the upper hybrid frequency $\omega_{UH} = (\omega_p^2 + \omega_c^2)^{1/2}$ where ω_p and ω_c are the electron plasma and gyro-frequencies, respectively. When the waves start growing, wave particle interaction causes diffusion of particles into the loss cone and the growth rate decreases until a steady state is reached where the collisional damping by the background plasma balances the growth. From this time onwards the energy density of the plasma waves falls to noise level, as no plateau is formed in two dimensional quasi-linear theory. However, if the particles diffusing into the loss cone are balanced by precipitation, it is possible to have continued loss cone distribution and a steady level of plasma waves could be maintained over long periods of time (e.g., over the lifetime of a moving type IV burst). Fundamental and harmonic radiations are generated by the plasma waves scattered from background ions or among themselves. Depending on the energy density of these plasma waves, one of them will dominate (Zaitsev and Stepanov, 1983). The upper hybrid waves are excited with phase velocities less than the thermal spread of the loss cone distribution. The waves are distributed isotropically in the plane perpendicular to the magnetic field. Therefore, the second harmonic emission is more efficient compared to the bump-on-tail case as the latter needs a secondary spectrum of plasma waves. The fundamental emission process is similar to the bump-on-tail case.

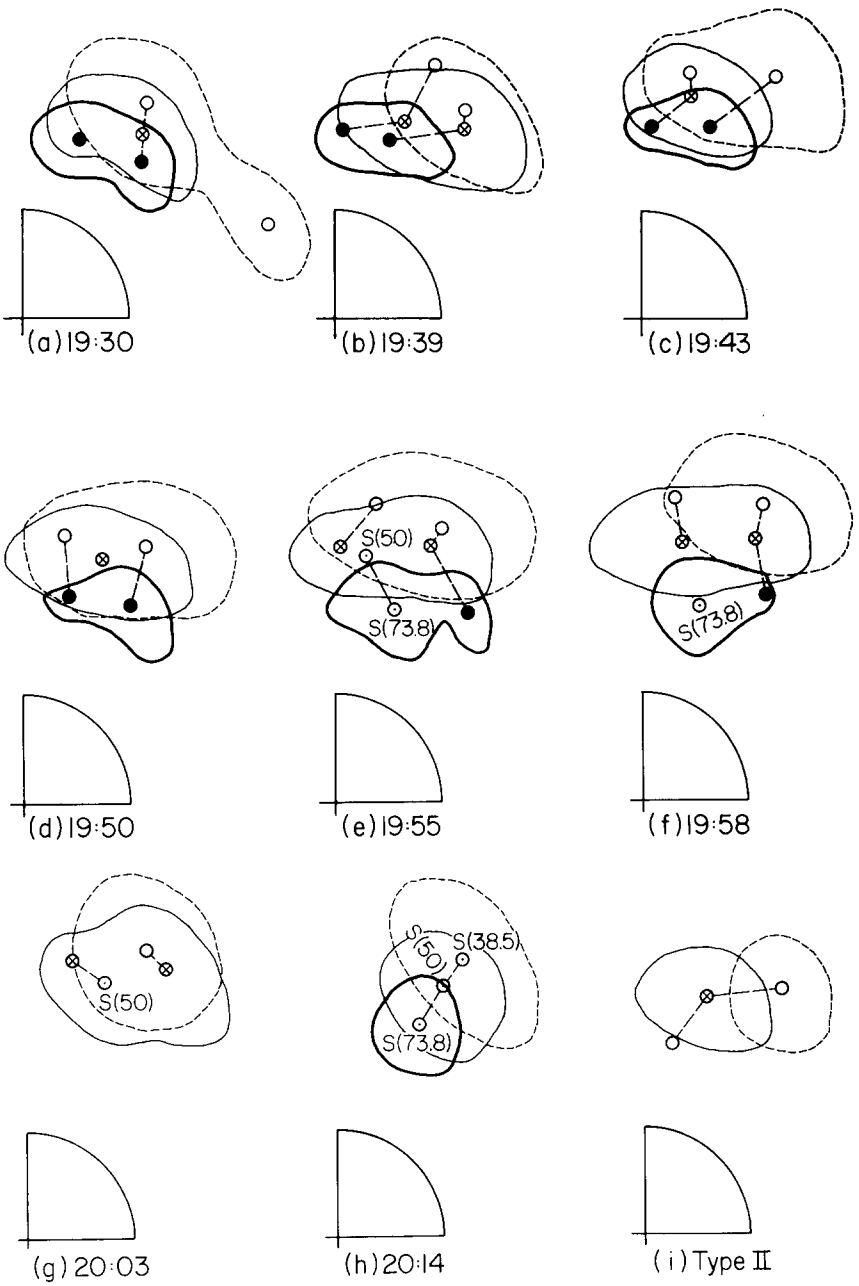

Fig. 10. The contours at 35% of peak brightness temperature and the centroids of the burst sources at different times. The thick solid, thin solid and dashed contours correspond to 73.8, 50, and 38.5 MHz radio bursts, respectively. Filled circles, circles with crosses and open circles represent the centroids of 73.8, 50, and 38.5 MHz bursts. The time of the burst is indicated on each figure. In (d), the 50 MHz source is due to the type II burst. From (e) onwards the stationary source also appeared, the centroid of which is marked by a circle with a dot and labelled *S* with the corresponding frequency in bracket. In (h), the moving sources have faded completely and only *S* sources are seen. In (i) the contours and centroids of type II burst are shown.

Various types of loss cone distributions have been considered in the literature (Zaitsev and Stepanov, 1983; Melrose, 1986) and all of them give nearly the same linear growth rate γ:

$$\gamma \simeq 0.1\omega_p \frac{n_L}{n_0} , \tag{2}$$

where n_L and n_0 are the densities of nonthermal and thermal electrons, respectively.

In steady state, the quasi-linear growth rate $\gamma_q \simeq \nu_{\text{eff}}/2$ where ν_{eff} is the effective collision frequency of the background plasma (see, e.g., Stepanov, 1974; Zaitsev and Stepanov, 1975). The quasi-linear growth rate depends on the density of the energetic particles and the details of the distribution function which is modified due to the back reaction of emitted upper hybrid waves. In general γ_q will be less than the linear growth rate γ. To obtain an order of magnitude estimate of the required density of nonthermal particles in the source, we use the linear growth rate as in Zaitsev and Stepanov (1983). In order that γ does not fall below collision rate, we need

$$\frac{n_L}{n_0} > 5\nu_{\text{eff}}/\omega_p = 3.2 \times 10^{-8} \quad \text{for} \quad \frac{\omega_p}{2\pi} = 25 \text{ MHz} . \tag{3}$$

Energy density of upper hybrid waves generated by the loss cone instability can be estimated by solving the quasi-linear equations. Stepanov (1974) solved them numerically and found that, unlike one-dimensional beam plasma instability, the loss-cone instability converts only about 10% of the energy of the nonthermal particles into wave energy (see also Zaitsev and Stepanov, 1975). The relative level (W) of plasma waves with respect to thermal energy density $n_0 T_0$ can, therefore, be written as

$$W = 0.1 \frac{n_L}{n_0} \frac{T_L}{T_0} , \tag{4}$$

where T_L and T_0 are the temperatures of nonthermal and thermal electrons, respectively. For $T_L/T_0 \sim 10^2$ and $n_L/n_0 \sim 10^{-8}$, $W \sim 10^{-7}$.

Plasma emission due to loss cone excited upper hybrid waves was calculated by Zaitsev and Stepanov (1983) to explain microwave emission. At low levels of plasma waves (as in the present case), the induced processes were found to be insignificant. Our calculations at meter wavelengths leads to the same conclusion. The resulting brightness temperatures due to fundamental (T_{b1}) and harmonic (T_{b2}) plasma emission are given by

$$T_{b1} = \frac{\pi}{36} \frac{\omega_p}{\nu_{\text{eff}}} \frac{v_\phi}{v_{t0}^2} T_0 W \tag{5}$$

and

$$T_{b2} = \frac{2(2\pi)^5}{15} \frac{c^4 n_0 T_0}{\omega_p^2 \nu_{\text{eff}} v_\phi} \frac{W^2}{X^2} , \tag{6}$$

where v_ϕ and v_{t0} are the phase velocity of the plasma waves and thermal velocity of background electrons; ν_{eff} is the electron ion collision frequency; c is the velocity of light and $X = (\Delta k)^3 c^3/\omega_p^3$ describes the effective range Δk of wave numbers over which the coalescence of upper hybrid waves takes place. Comparing (5) and (6) we see that

$$\frac{T_{b1}}{T_{b2}} = 6.25 \times 10^{-12} X^2, \tag{7}$$

where we have considered emissions at 50 MHz and assumed values $v_\phi \sim 2 \times 10^9$ cm s^{-1}, $v_{t0} \sim 4 \times 10^8$ cm s^{-1}, and $W \sim 1.65 \times 10^{-7}$. Equation (7) implies that for $X^2 < 1.6 \times 10^{11}$ or $\Delta k < k_e$ (where k_e is the Debye wave number) the second harmonic emission is brighter than the fundamental. However, fundamental emission can take place only when the density in the source region is high enough.

In order to check the density in the source region of moving type IV burst, we need simultaneous radio and white-light observations. The only time both the CME and the moving type IV are observed simultaneously is at 19:39 UT, as seen in Figure 7(b). Since the moving type IV source at 50 MHz lies exactly on the CME, the density in the source can be obtained from the column density scans of the CME. The errors in the column density measurements due to various effects are estimated to be 10–20% (Burkpile, 1988, private communication). The column densities are obtained, assuming that the scattering electrons are in the plane of the sky. If the CME is also $\sim 30°$ away from the plane of the sky, the error introduced in the column density does not exceed the total errors from other sources mentioned above. From Figure 11 we see that the maximum column density at a height of 2.3 $R_\odot$ (corresponding to the height of 50 MHz moving type IV burst) is $\sim 2 \times 10^{17}$ cm^{-2}. The FWHM is $\sim 0.33\ R_\odot$ corresponding to the loop thickness. If we take this also to be the depth of the loop along the line-of-sight, then the plasma density in the loop becomes $\sim 8.5 \times 10^6$ cm^{-3}. This is smaller by a factor of ~ 3.5 than the density needed for fundamental emission at 50 MHz, whereas the density is sufficient to produce harmonic emission. Unfortunately, the next CME observation is only after the moving source has completely faded out and so we cannot check the source density at higher locations of the moving type IV source. As the harmonic emission seems likely, let us estimate the brightness temperature. Substituting $\omega_p/2\pi = 25$ MHz (so that $n_0 = 8.0 \times 10^6$ cm^{-3}), $v_\phi \sim 2 \times 10^9$ cm s^{-1}, $\nu_{ei} = 1.0$ s^{-1}, $T_0 = 10^6$ K, $W = 1.65 \times 10^{-7}$, and $(\Delta k)^3 \sim 0.78 k_e^3$ in Equation (6), we get $T_{b2} = 4.2 \times 10^7$ which is close to the observed peak brightness temperature of $\sim 2 \times 10^7$ K at 50 MHz. Here we have ignored the effects of inhomogeneities (White, Kundu, and Szabo, 1986) in the source region which results in a larger apparent source size than the true size so that the actual brightness temperature may be higher. Higher T_b needs a lower Δk.

An estimate of the magnetic field in the source region can be made if the polarization of the moving type IV burst is known. We do not have polarization information. In general it is known that only the isolated source variety of moving type IV bursts shows very high polarization (Robinson, 1978). Stepanov (1974) assumed that the plasma

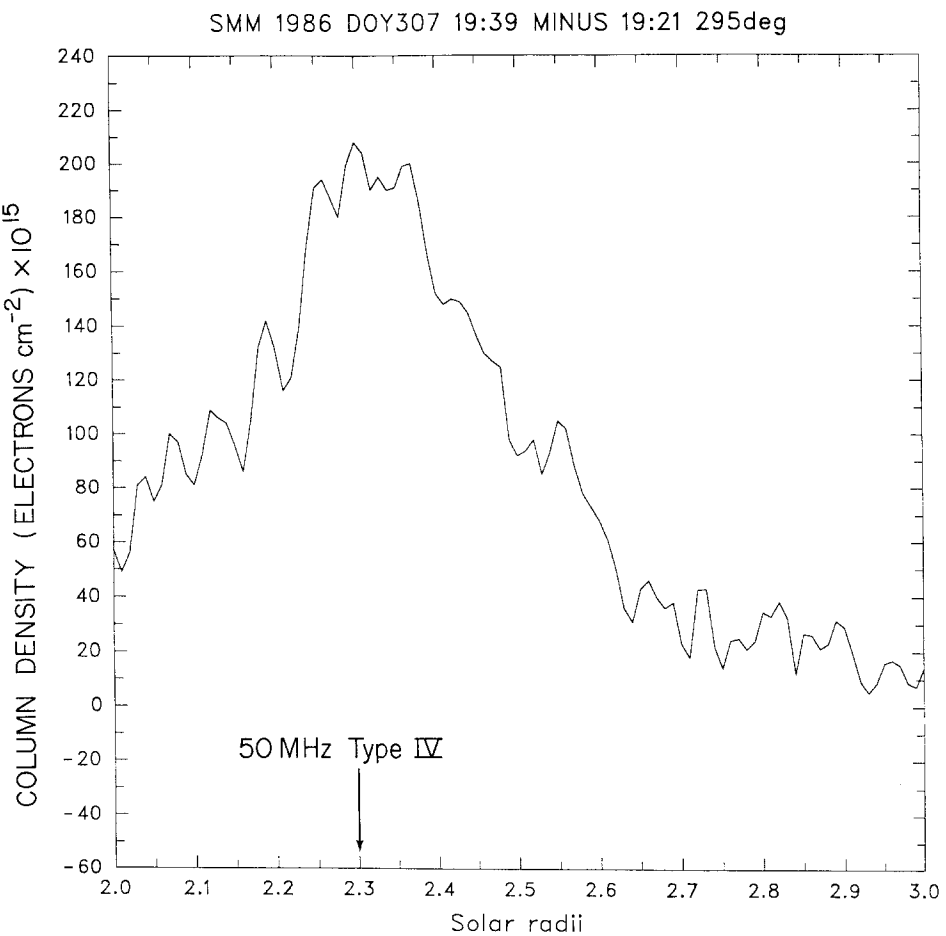

Fig. 11. Column density radial scan at the position angle of the moving type IV burst at 50 MHz. The peak corresponds to the loop. Height of the moving type IV burst centroid is marked.

frequency is very close to the gyrofrequency ($\omega_p^2 \leq 1.25\omega_c^2$) in order to obtain high polarization. But this assumption leads to an unrealistically high magnetic field. For example, second harmonic plasma emission at 50 MHz corresponds to a magnetic field of ~ 8 G which is rather high value for the corona at metric heights. It is believed that in the metric corona the plasm frequency exceeds the gyrofrequency (Melrose, 1980). If the high polarization requirement is relaxed, then the largest magnetic field required is for the case where the upper hybrid frequency resonates with the fourth harmonic of the gyrofrequency. This corresponds to $\omega_p^2 = 15\omega_c^2$ so that we get a magnetic field of ~ 2.3 G and becomes < 1 G for resonance with sixth harmonic.

5. Summary and Conclusions

(i) Using simultaneous multifrequency observations we were able to understand several aspects of the radio emission associated with a loop-type CME. A fairly good under-

standing of the event could be obtained using various types of metric emissions even though most of the near surface activities are occulted. Our observations are consistent with the result that the CME and moving type IV lift off is several minutes before the associated flare.

(ii) The type II burst is located close to or behind the moving type IV burst, even though they have nearly the same speed. This suggests that the shock might not have been driven by the mass ejection. The shock might have originated due to flare explosion (decoupled shock), the flare itself being indicated by the early type III bursts. Therefore, the temporal coincidence between CME and type II bursts may not indicate a cause and effect relation between them.

(iii) Particle acceleration takes place during the impulsive phase of the flare (indicated by early type III bursts) and also in the shock waves. If conditions are appropriate, both these processes can supply energetic particles to the CME to produce the observed moving type IV bursts.

(iv) The structure of the magnetic loop emitting moving type IV bursts in metric wavelengths can be traced to great heights (up to $\sim 4.5\, R_\odot$) in the corona. The radio sources are situated along both legs of the loop, lower frequency occurring at a greater height. The radio emission can be explained by second harmonic plasma emission, the plasma waves at the upper hybrid frequency being generated by electrostatic loss cone instability of electrons trapped in the magnetic arch. The plasma emission requires electron energies similar to the type III electrons (tens of keV). Nonthermal particle densities as small as 10^{-8} times the background density seems to be adequate. The plasma density obtained from column density of the mass ejection measured in white light is found to be adequate to generate the observed emission. To get reasonable estimate of the magnetic field in the moving type IV source region, the plasma frequency has to exceed the gyrofrequency by a factor of ~ 4. The resulting magnetic field is $\lesssim 2$ G.

Acknowledgements

We thank Dr S. M. White for critical reading of the manuscript and many helpful suggestions. We thank Dr A. J. Hundhausen for providing the SMM-C/P data and comments on a draft of this paper. Ms Joan Burkpile generated the SMM-C/P images in various forms which were extremely useful in our analysis and we gratefully acknowledge her help. We thank Dr C. Garcia for the HAO's Mauna Loa *K* coronameter data. Partial computational support was provided by the University of Maryland Computer Science Center. The useful comments of the anonymous referee are gratefully acknowledged. This research was supported by the NSF grant ATM 88–16008.

References

Burkpile, J.: 1988, private communication.
de Jager, C.: 1986, *Space Sci. Rev.* **44**, 43.

Duncan, R. A.: 1979, *Solar Phys.* **63**, 389.
Duncan, R. A.: 1981, *Solar Phys.* **73**, 191.
Gary, D. E., Dulk, G. A., House, L. L., Illing, R., Wagner, W. J., and McLean, D. J.: 1985, *Astron. Astrophys.* **152**, 42.
Gopalswamy, N. and Kundu, M. R.: 1987a, *Solar Phys.* **114**, 347.
Gopalswamy, N. and Kundu, M. R.: 1987b, *Solar Phys.* **111**, 347.
Gopalswamy, N., Kundu, M. R., and Szabo, A.: 1987, *Solar Phys.* **108**, 333.
Harrison, R. A., Wagget, P. W., Bentley, R. D., Phillips, K. J. H., Burner, M., Dryer, M., and Simnett, G. M.: 1985, *Solar Phys.* **97**, 387.
Kundu, M. R. and Gopalswamy, N.: 1987, *Solar Phys.* **112**, 133.
Kundu, M. R., Erickson, W. C., Gergely, T. E., Mahoney, M. J., and Turner, P. J.: 1983, *Solar Phys.* **83**, 365.
Kundu, M. R., Gopalswamy, N., Saba, J. L. R., Schmelz, J. T., and Strong, K. T.: 1988, *Solar Phys.* **114**, 273.
Lin, R. P., Potter, D. W., Gurnett, D. A., and Scarf, F. L.: 1981, *Astrophys. J.* **251**, 364.
McCabe, M.: 1987, private communication.
Melrose, D. B.: 1975, *Solar Phys.* **43**, 211.
Melrose, D. B.: 1980, *Space Sci. Rev.* **26**, 3.
Melrose, D. B., and Brown, J. C.: 1976, *Monthly Notices Roy. Astron. Soc.* **176**, 15.
Robinson, R. D.: 1978, *Solar Phys.* **60**, 383.
Robinson, R. D.: 1985, in *Solar Radio Physics*, Cambridge Univ. Press, Cambridge, Ch. 14, p. 385.
Schmahl, E. J. and Hildner, E.: 1977, *Solar Phys.* **55**, 473.
Stepanov, A. V.: 1974, *Soviet Astron.* **17**, 781.
Stewart, R. A., Dulk, G. A., Sheridan, K. V., House, L. L., Wagner, W. J., Sawyer, C., and Illing, R.: 1982, *Astron. Astrophys.* **116**, 217.
Suzuki, S. and Dulk, G. A.: 1985, in *Solar Radio Physics*, Cambridge University Press, Cambridge, Ch. 12, p. 289.
Suzuki, S. and Sheridan, K. V.: 1982, *Proc. Astron. Soc. Australia* **4**, 382.
Wagner, W. J.: 1985, in C. de Jager and C. Biao (eds.), *Proceedings of Kunming Workshop on 'Solar Physics and Interplanetary Travelling Phenomena'*, Kunming, China, Vol. II, p. 978.
White, S. M., Kundu, M. R., and Szabo, A.: 1986, *Solar Phys.* **107**, 135.
Zaitsev, V. V. and Stepanov, A. V.: 1975, *Astron. Astrophys.* **45**, 135.
Zaitsev, V. V. and Stepanov, A. V.: 1983, *Solar Phys.* **88**, 297.